

# Light-driven flipping of azobenzene assemblies — sparse crystal structures and responsive behaviour to polarized light

Yoshiyuki Kageyama<sup>\*a</sup>, Tomonori Ikegami<sup>b</sup>, Shinnosuke Satonaga<sup>b</sup>, Kazuma Obara<sup>b</sup>, Hiroyasu Sato<sup>c</sup>, and Sadamu Takeda<sup>\*a</sup>

<sup>a</sup> Department of Chemistry, Faculty of Science, Hokkaido University, Sapporo, 060-0810 (Japan)  
E-mail: y.kageyama@sci.hokudai.ac.jp stakeda@sci.hokudai.ac.jp

<sup>b</sup> Graduate School of Chemical Sciences and Engineering, Hokkaido University, Sapporo, 060-0810 (Japan)

<sup>c</sup> Rigaku Corporation, Akishima, 196-8666 (Japan)

## Abstract

For creation of autonomous microrobots which are able to move under conditions of a constant environment and a constant energy supply, a mechanism for maintenance of mechanical motion with a capacity for self-control is required. This requirement is known as self-organisation. The latter concept represents the ability of a system to evade equilibrium through formation of a spatio-temporal pattern which is realized with the existence of a continuously-working energy converter and cooperatively-working factors. Following our previous finding of a light-powered, self-oscillatory flipping motion of a co-crystal of oleic acid and an azobenzene derivative, we present here regulation of the flipping motion by a light-receiving sensor molecule in relation to the alignment and role of azobenzene molecules in co-crystal and single-component crystals of azobenzene. A single crystal structure analysis revealed a mille-feuille-like layered structure of sparse and dense layers of six independent azobenzene moieties. In the anisotropic structure, a specific azobenzene molecule acts as a reaction center for the conversion of light to a mechanical function process, while the other molecules act as modulators for spatio-pattern formation. Due to the photoisomerisation processes of the azobenzene molecules, path selection for different cyclic motions is observed according to the polarisation state of incident light. In addition to clarifying the molecular integration structure for inducing self-organized mechanical behavior, the present results demonstrate that autonomously drivable molecular materials can exhibit information-responsive, self-sustainable motion by incorporating stimulus-responsive sensors. Thus, a design guideline for the construction of self-governable molecular robots is presented.

## Introduction

Two key characteristics of living systems are a form of metabolism and energy dissipation.<sup>1</sup> Self-governed functions of living things are powered by chemical processes at the molecular level which consume externally supplied energy and are self-controlled in response to external conditions. An ongoing research goal has been to mimic this characteristic feature of living systems

with synthetic materials. An application of this advance would be the creation of autonomous molecular robots and machines which are able to work independently and repair themselves.<sup>2,3,4</sup> However, there is a fundamental difference between stimulus-responsive materials and life-like autonomous systems.<sup>5</sup> For example, deformation of a stimulus-responsive material involves dynamics which approach an equilibrium state (e.g., a static structure) under stimulus conditions. Such materials then require external information (e.g., environmental changes) to discharge the received energy and sustain repetitive motion. In contrast, autonomous systems automatically discharge received energy for their self-sustainable functions and they convert accepted input into a spatio-temporal pattern.

Thus, it has been proposed that the first step for synthesis of self-governed behaviour at a multi-molecular level is to maintain a system out-of-equilibrium. To this end, characterization of reactions involving molecular assemblies<sup>6,7,8</sup> and assembly-catalysed triangular reactions<sup>9</sup> have recently been proposed. However, these near-equilibrium behaviours are insufficient for generating mechanical functions. The second and third steps needed to synthesize autonomous-working molecular systems are to realize mechanical motion apart from thermodynamic equilibrium and to incorporate external information for self-maintenance behaviour.

### **Anisotropic structure for light-responsive materials**

Alignment of catalysts or photochromic molecules for the purpose of creating chemical-fueled or light-powered autonomous and mechanical-working materials is a current challenge in chemistry.<sup>10</sup> <sup>11</sup> To date, various light-responsive materials have been characterized. For example, a polymer gel which achieves an earthworm-like crawling motion in response to a traveling light has been developed by Ishida et al. based on an alignment of titanate-nanosheets and gold-nanoparticles.<sup>12</sup> Fukushima and co-workers have induced a bending motion in an azobenzene polymer brush via alignment of a sensitizer in response to non-polarised light.<sup>13</sup> Meanwhile, Katstonis and co-workers have demonstrated a spring-like transformation of an azobenzene liquid crystalline polymer.<sup>14</sup> These studies which incorporate anisotropic structures of materials are in stark contrast to early-stage light-responsive polymers which do not undergo morphological changes without application of polarized light.<sup>15</sup> Meanwhile, stimulus-responsive liquid crystals have also been characterized. These well-organized crystals exhibit functional morphological changes based on their molecular assembly behavior.<sup>16-23</sup> Similarly, reversible macroscopic transformations of crystals have been reported to date.<sup>24-28</sup>

### **Sustainable motion**

Except for a few examples of chemical oscillation systems,<sup>29,30</sup> stimulus-responsive materials generally repeat their motions in response to an externally controlled stimulus.<sup>12-28</sup> To achieve motion that repeats without external controls, researchers have tried to employ time-delayed cooperative effects.<sup>31-40</sup> These effects derive from adjustments in the relative direction between energy sources and receptive objects. For example, the amount of the energy received can be tuned by deformation of the objects.<sup>4</sup> In this manner, continuous translations<sup>31-35</sup> or oscillations<sup>36-40</sup> under anisotropic-restricted conditions have been successful. To achieve fully autonomous motions without adjusting external information (e.g., direction of the stimulus source), another “quality” of

molecular association is required: cooperation of asymmetric processes to enable materials to evade a static steady state.<sup>4,41</sup>

### **Light-powered self-sustainable flipping motion of a crystalline assembly of an azobenzene derivative**

Recently, we observed the self-oscillatory flipping motion of a co-crystal of an azobenzene derivative (**1**: 6-[4-(4-*n*-butylphenylazo)phenoxy]hexanoic acid) and oleic acid (**2**) (Figure 1).<sup>42</sup> The autonomous sustainable motion in this crystal is due to immanent self-organisation of azobenzene photoisomerisation events and a crystalline phase transition (Figure 2). Briefly, a *trans*-to-*cis* photoisomerisation event occurs which leads to a change in the isomer ratio of azobenzene to trigger a crystalline phase transition to a secondary structure. A *cis*-to-*trans* photoisomerisation event subsequently occurs and a returning of the isomerisation ratio provokes a phase transition back to the original structure. Switching of reaction direction is the result of a sudden change in photoreaction kinetics due to realignment. Due to the specific isomer ratios for the phase transitions and the determined molecular arrangement in each state, oscillation occurs in a limit-cycle manner with four limit sets. Such limit-cycle self-oscillatory dynamics are fundamental for attaining autonomous energy conversion.<sup>43</sup> While molecular ordering and re-ordering are key for periodic dynamics, we were unable to determine the crystal structure of the soft co-assembly of **1** and **2**. However, it was assumed that the crystal had a lamellar structure based on one-dimensional powder X-ray diffraction (1D-XRD) data.

Herein, we report our successful realisation of the self-sustainable flipping motion of a single component crystal of **1** without **2**, for which a crystal structure was determined. We also describe our understanding of the self-oscillatory capacity of the **1** and **2** co-crystal, as well as the influence of external information to self-governing materials (e.g., motions under polarised light). In the crystal, a part of the azobenzene converted light-energy to periodic mechanical motion of crystal by its repetitive photoisomerization, and other azobenzene modulated the pattern of the motion in response to polarization angle of the light. The mechanical motion, a combination of autonomous-drive and sensing, can be viewed as a drone-type robotic behaviour.

In total, we report four distinct crystals. 1) **SC** is a single component crystal of **1** and it exhibits self-oscillatory flipping motion under blue-light irradiation in phosphate-buffered water. 2) **EC** is a single component crystal of **1** which is obtained with recrystallisation of **1** from EtOH and it does not exhibit light-responsive mechanical motion. 3) **NC** is a single component crystal which is obtained from hot phosphate-buffered water and it also does not exhibit light-triggered flipping motion. 4) Co-crystal (**coC**) refers to the previously reported self-oscillatory co-crystal composed of **1** and **2**, and it has an approximate ratio of 6:4.<sup>42</sup>

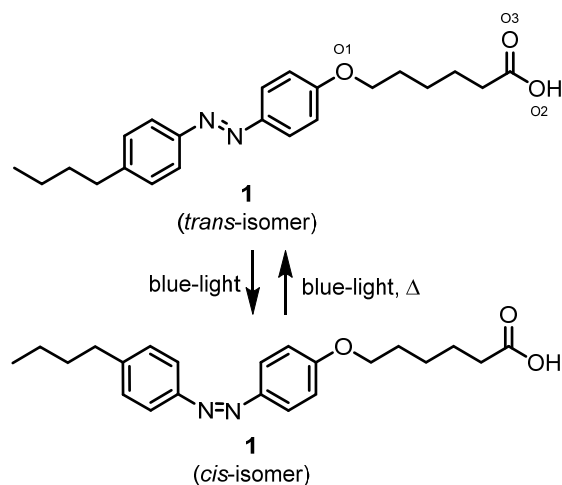


**Figure 1.** Schematic illustration of an azobenzene derivative (**1**) and its photoisomerisation. Atomic labels derive from single-crystal XRD analysis (Figure 6a).

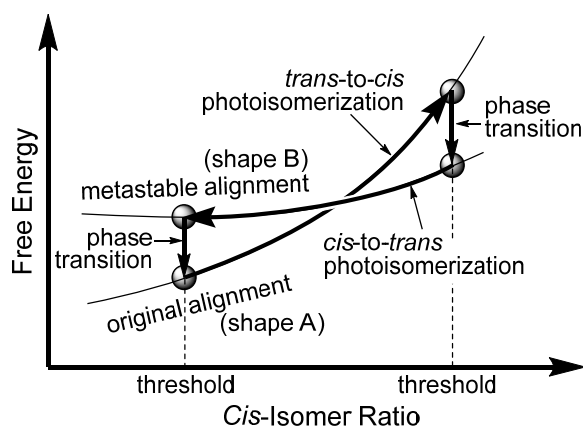


**Figure 2.** Schematic diagram of the limit-cycle self-oscillation of an azobenzene-containing crystal under blue-light as predicted from previous results.<sup>42</sup>

## Experimental Section

### General

The azobenzene derivative (**1**) used was synthesised according to a previously described method.<sup>19,20</sup> Sodium oleate (Tokyo Chemical Industrial Co., Ltd., Japan), sodium dihydrogen phosphate and disodium hydrogen phosphate (Nacalai Tesque Inc., Japan), and distilled water (Fujifilm Wako Chemical Ltd., Japan) were purchased and used without further purification. A D8 Advance (Bruker, Germany), Miniflex600 (Rigaku, Japan) or RINT2000 (Rigaku, Japan) system was used to measure 1D-XRD. To observe light-powered motion in the crystals, either a differential interference contrast (DIC) microscope equipped with a mercury lamp epi-fluorescent unit (Nikon TE2000, Japan) or a DIC microscope equipped with an Intensilight epi-fluorescent illuminator (Nikon Ti-U, Japan) was used. To select the colour of the incident light, filter units (Nikon BV-1A for

435-nm irradiation and Nikon B-2A for 470-nm irradiation) were used. Light power was controlled with neutral density filters according to a previously described method.<sup>42</sup> To observe motion under polarised light irradiation, the TE2000 system was used with a BV-1A filter and a polariser inserted below the lens-revolver, generally without using DIC optics.<sup>44</sup> The tilt angle of the polarisation plane from the horizontal direction in the captured image was measured as counter clockwise. Image-Pro Premier software (Media Cybernetics, USA) was used to analyse motion. For component analysis by high-performance liquid chromatography (HPLC), a LC2000 series system (JASCO, Japan) equipped with a ODS column (Cosmosil 5C18ARII, Nacalai Tesque Inc, Japan) was used. A 9:1 mixture of MeOH and 0.05% TFAaq was used as the eluent. Light absorbance was recorded at 416-nm, the wavelength at which the absorption coefficients of the *trans*-isomer and *cis*-isomer of **1** are equal in the same solvent.<sup>42</sup>

### Preparation of crystals

*Preparation of 1 (SC) crystals.* In a glass vial, 50 mM NaOH aq (288  $\mu$ L) was added to 5.3 mg of **1** (14.4 mmol). The mixture was shaken to form a viscous dispersion. Next, 5.0 mL of 75 mM phosphate-buffered water (pH 7.2, prepared by mixing Na<sub>2</sub>HPO<sub>4</sub> and NaH<sub>2</sub>PO<sub>4</sub>) was added. The solution was just heated to boiling on a hot plate and then was cooled at room temperature. **SC** was obtained with other polymorphic crystals. For microscopic observation, the sample was placed on a glass slide and sealed with a frame-seal incubation chamber (Bio-Rad). To obtain 1D-XRD measurements, sediment from the dispersion was placed in the sample chamber.

*Preparation of 1 (NC) crystals.* A round-bottom flask containing 50 mM NaOH aq (1.73 mL) and 31.9 mg of **1** (86.6  $\mu$ mol) was shaken to form a viscous dispersion. Thirty mL of 75 mM phosphate-buffered water (pH 7.2, prepared by mixing of Na<sub>2</sub>HPO<sub>4</sub> and NaH<sub>2</sub>PO<sub>4</sub>) was subsequently added. The mixture was kept at 85 °C by an oil-bath. After 4 h, the hot dispersion mixture was transferred into a light shielding glass vial and cooled at room temperature. After 20 h, microscopic observations and 1D-XRD measurements were collected.

*Preparation of 1 and 2 crystals (coC).*<sup>42</sup> In a glass vial, 50 mM NaOH aq (288  $\mu$ L) was added to 5.3 mg of **1** (14.4 mmol). The mixture was shaken to form a viscous dispersion before 6.6 mg sodium oleate (sodium salt of **2**, 21.6 mmol) and 5.0 mL of 75 mM phosphate-buffered water (pH 7.5, prepared by mixing of Na<sub>2</sub>HPO<sub>4</sub> and NaH<sub>2</sub>PO<sub>4</sub>) were added. This mixture was subsequently heated to 55 °C, was ultrasonicated for 30 min, and then was cooled to room temperature under dark conditions. Crystals of **coC** were obtained.

### Single crystal XRD measurements

Single crystal XRD measurements for **SC** were performed with a Rigaku XtaLAB P200 instrument with Cu-K $\alpha$  radiation ( $\lambda = 1.54184$  Å) applied at 93 K. Measurements for **EC** were performed with a Rigaku XtaLAB AFC12 instrument with Cu-K $\alpha$  radiation ( $\lambda = 1.54184$  Å) applied at 293 K. Collected data were integrated, corrected, and scaled with the CrysAlis<sup>Pro</sup> program package. The structure was solved by direct methods (SHELXT Version 2014/4) and refined by the full-matrix least-squares method on  $F^2$  for all reflections (SHELXL-2017/1). All hydrogen atoms were placed according to AFIX instructions. All non-hydrogen atoms were anisotropically refined. Electron densities for the molecules in **SC** were obscured due to thermal motion and disordering. Therefore, the electron density map for **SC** was refined by applying certain restraints (DFIX, DANG, RIGU, ISOR). Cif-files

were deposited in CCDC1833361 for **EC** and in CCDC1833362 for **SC**. These can be obtained free of charge at [www.ccdc.cam.ac.uk/structures](http://www.ccdc.cam.ac.uk/structures). The powder patterns displayed in Figures 3b and 3c were generated with Mercury 3.7 software.

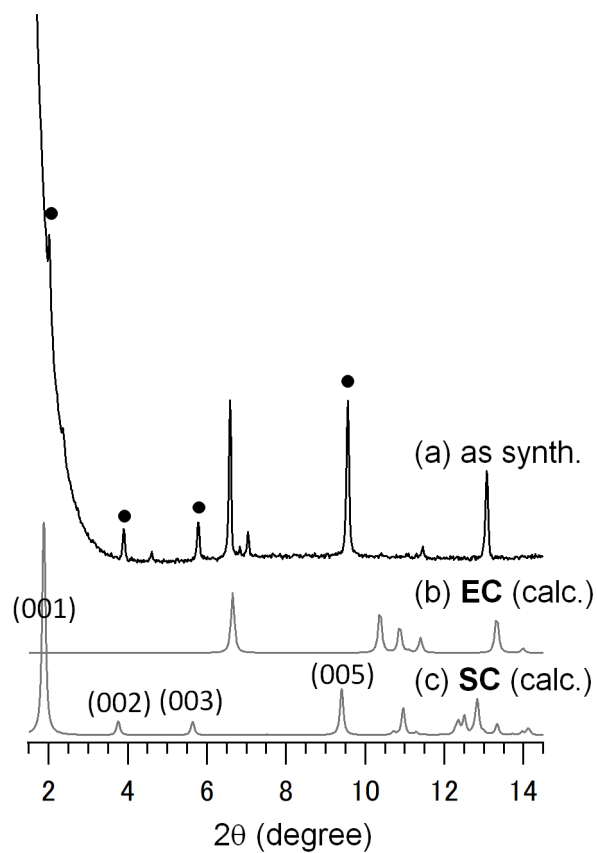
#### Calculation of transition dipole moments

Geometry optimisation of the molecular structures in the crystal was performed by applying a molecular dynamics calculation, without changing the unit cell, with the Forcite module in Materials Studio (BIOVIA, Accelrys) and a CompassII force field. Single crystal XRD analysis provided the initial atomic coordinates for the force field calculation. Transition dipole moments for photo-excitations of each azobenzene molecule in **SC** were then estimated individually by using Gaussian 16 software<sup>45</sup> with the TD-B3LYP/6-31+G(d) level of theory. The transition dipole moments which were obtained include considerable inaccuracies due to the highly disordered nature of the crystal structure analyzed. The wavelengths for the lowest transitions were calculated to be: 485 nm, 480 nm, 482 nm, 492 nm, 492 nm, and 481 nm for molecules A-F in the crystal, respectively. These molecules are labelled with different colours in Figure 6.

## Results and Discussion

#### Self-oscillatory motion of **SC**

After cooling a boiled solution of **1**, **SC** was obtained as an aqueous dispersion with other polymorphic crystals. The 1D-XRD pattern of the sediment from this dispersion is shown in Figure 3. One of the polymorphic crystals showed the same structure as **EC**. When the dispersion was warmed to 60 °C and then cooled, **EC** formed predominantly. Alternatively, when the dispersion was heated to approximately 85 °C for 4 h and then was incubated overnight at room temperature, **NC** was predominantly obtained [Figure S1 in Electronic supplementary information (ESI)]. According to these results, **SC** is assumed to be a kinetically-trapped polymorph of **1**. It was difficult to avoid the formation of crystal polymorphs to obtain **SC**. This may be due to the assembling pathways of amphiphilic carboxylic acids in neutral pH water being complicated as a result of fluctuations in acid-dissociation dynamics under inhomogeneous conditions and less-selective interactions between alkyl chains.<sup>46</sup> In contrast, preparation of **coC** (*vide infra*) was more straightforward.<sup>42</sup> When the mixed dispersion solution containing **SC** and other polymorphs was sealed between glass slides and viewed with a DIC microscope, **SC** was observed as a curled plate crystal. Next, non-polarised continuous-wave blue-light was used to irradiate **SC**. For these experiments, a high-pressure mercury arc lamp with band-pass filters installed in the microscope was used. A self-oscillatory flipping motion was observed under 435-nm and 470-nm light (illustrated in Figure 4 and shown in Movies S1-4 in ESI).<sup>42,47</sup> However, blue-light irradiation did not induce morphological changes in **EC** and **NC** crystals.

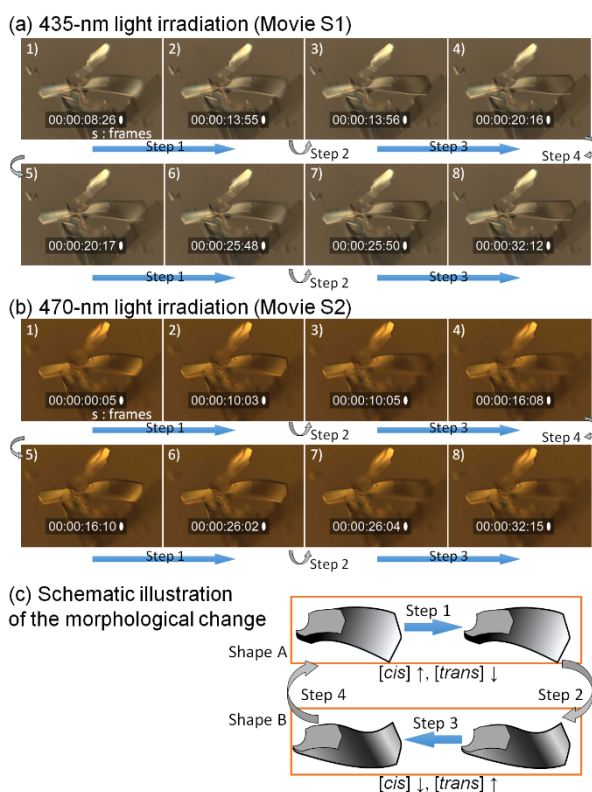


**Figure 3.** A powder XRD (pXRD) instrument was used to measure 1D-XRD patterns under aqueous conditions from single-crystal XRD analyses. (a) An as-prepared sample of **1** (**SC**) (e.g., a mixture of polymorphs; filled circles indicate diffractions from **SC**) was subjected to 1D-XRD. (b) Calculated pXRD pattern for a crystal of **1** (**EC**). (c) Calculated pXRD pattern for a crystal of **1** (**SC**) with indication of Miller indices.

---

**Table 1.** Comparison of **coC** and **SC**.

Characteristic	coC <sup>42</sup>	SC
Crystal Formation	Formed as single morphology by cooling an aqueous solution of <b>1</b> and oleic acid from a moderate temperature (~55 °C)	Formed as polymorph crystals following cooling of a boiled aqueous solution of <b>1</b>
Shape of Crystal	Clean-cut flattened shape	Curled plate shape
Oscillatory Cycle	Bending and unbending motion in 4 steps	Curling and uncurling motion in 4 steps
Phase Transition Period	Steps 2 and 4	Steps 2 and 4
Photoisomerisation Period	Step 1 ( <i>cis</i> -isomer increasing) and Step 3 ( <i>cis</i> -isomer decreasing)	Step 1 ( <i>cis</i> -isomer increasing) and Step 3 ( <i>cis</i> -isomer decreasing)
pXRD	Figure S1 in ESI (single morphology)	Figure 3a (polymorphs)
Small-Angle pXRD	$d = 4.6$ nm (in darkness) $d = 4.0$ nm (under 455-nm light)	$d = 4.6$ nm (in darkness) $d = 4.6$ nm (under 450-nm light): only the original diffraction was captured
Single-Crystal XRD	Not resolved	Refined (Figure 6); CCDC1833362
<i>Cis</i> -isomer Ratio in PSS (including large errors)	3.5% under 455-nm LED light	4.8% under 435-nm light (Figure S6 in ESI)

**Figure 4.** Sequential DIC micrographs of **SC** (a) under continuous 435-nm light irradiation (Movie S1) and (b) under continuous 470-nm light irradiation (Movie S2). A schematic illustration is provided for each step of the oscillatory motion observed.

The time profile obtained for the oscillatory motion of **SC** was similar to that of **coC**, although the flipping motion occurred as twisting along the face of the curly crystal. As shown in Figures 5a (Movie S1 in ESI) and 5b (Movie S2 in ESI) for the motions under 435-nm and 470-nm light, respectively, one cycle of oscillation consisted of four steps: sluggish bending (Step 1), rapid flipping (Step 2), sluggish unbending (Step 3), and rapid reverse flipping (Step 4). The crystal repeated this regular cyclic motion with light power-dependent frequency. Duration times of Steps 1 and 3 ( $\tau_1$  and  $\tau_3$ , respectively) depended on the power and wavelength of the light applied. The logarithm of  $1/\tau_1$  and  $1/\tau_3$  were plotted as a function of the logarithm of light power in Figure 5c. Each slope in the plot is 1, indicating that Steps 1 and 3 are photoinduced self-exciting processes with a crucial number of photons. Photoisomerisation continues during these steps until the isomer ratio reaches a certain threshold at which transitions to Steps 2 and 4 occur, respectively. In contrast, the duration and amplitude of Steps 2 and 4 remain constant while the intensity and wavelength of the irradiation applied changes. Based on our previous discussion,<sup>42</sup> we can infer that these steps represent processes of a crystalline phase transition. Therefore, we conclude that the self-oscillatory flipping of **SC**, similar to that of **coC**, is established by successively alternating steps of isomerisation (Steps 1 and 3) and phase transition (Step 2 and 4) (Figure 2). Furthermore, as the  $\tau_1/\tau_3$  ratio is greater under 470-nm light than under 435-nm light,<sup>48</sup> we also conclude that the photoreaction process to increase (or decrease) the population of *cis*-isomer occurs in Step 1 (or Step 3).

It is noteworthy that more complicated flipping motions with multi-mode oscillations were also frequently observed (Movie S5 in ESI). We will discuss this observation below.

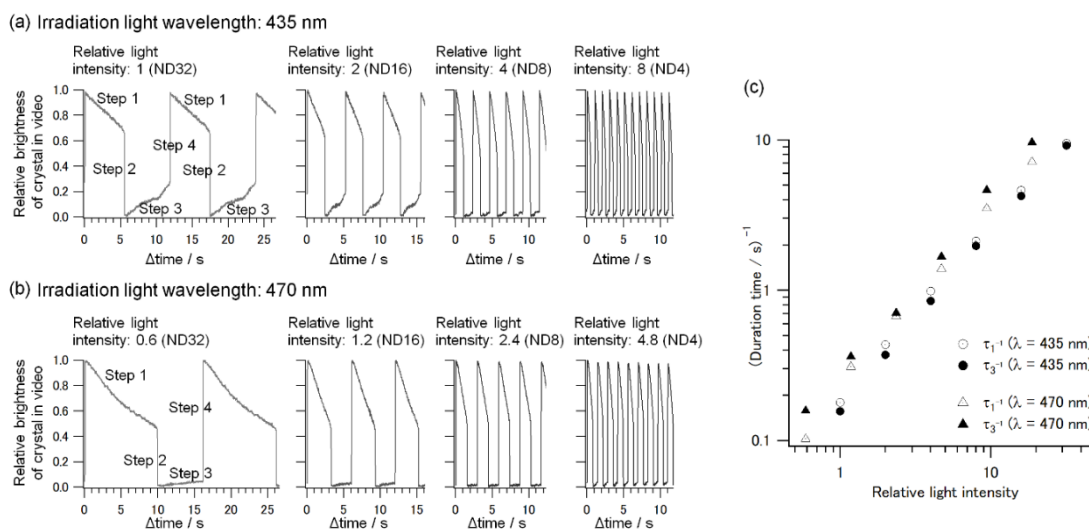


**Figure 5.** Time profiles of oscillatory motion of **SC** (a) under continuous 435-nm light irradiation (Movie S1 in ESI) and (b) under continuous 470-nm light irradiation (Movie S2 in ESI). Several different powers of light were obtained by using neutral density filters. In addition, light power of the 470-nm light was 0.6-fold that of the 435-nm light. Horizontal axes were defined by the brightness of the crystal face in the raw source data of Movies S1 and S2 in ESI, as evaluated by using Image Pro Premier software. Amplitudes of the change in relative brightness differed between 435-nm light and 470-nm light because different filter units were used to record the movies under each wavelength. (c) Light-intensity dependencies of the duration times. The horizontal axis was standardised by the incident energy (Watt) under 435-nm light with a pair of ND8 and ND4 filters.

### Molecular ordering in SC

Clear small-angle pXRD patterns were previously observed in both original and secondary alignments of **coC**.<sup>42</sup> However, we were unable to refine these crystal structures by performing a single-crystal XRD analysis. In contrast, we were able to obtain the crystal structure of **SC** by using single-crystal XRD measurements at 93 K. The residual factor was 26.3%, primarily due to the highly disordered soft structure of **SC** (Table 2). As shown in Figures 6a and 6c, six independent molecules exist in a unit cell with a *P1* space group. The relationship between cell-axis and the shape of the investigated crystal is shown in Figures 6b and 6c. All of the carboxyl groups contribute to form a dimer structure and they are also in close proximity with four oxygen atoms of ether groups (O1B, O1C, O1E, and O1F) from different molecules (Table 3). Displacements of atoms near the carboxyl groups and the four ether oxygens are smaller than those of the other atoms present. In addition, displacements of all of the atoms in **SC** are larger than the atom displacements in **EC**, a crystal which was measured at room temperature (Figure S3 in ESI). The crystal packing of **SC** (Figure 6d) shows a unique layer-by-layer structure, with alternating layers having moderate (green) or large (red) atomic displacements. Interactions between carboxyl dimers and neighbouring ether oxygens (O1B, O1C, O1E, and O1F) appear to induce the formation of durable skeletal layers (green), while less-polar groups are loosely stacked between the skeletal layers (red).

**Table 2.** Crystallography data for **SC** and **EC**.

Characteristic	<b>SC</b>	<b>EC</b>
Temperature	93 K	Room Temp.
Molecular Formula	C <sub>22</sub> H <sub>28</sub> N <sub>2</sub> O <sub>3</sub>	C <sub>22</sub> H <sub>28</sub> N <sub>2</sub> O <sub>3</sub>
Crystal system	Triclinic	Triclinic
Space group	<i>P1</i>	<i>P-1</i>
Unit cell length		
<i>a</i> / Å	7.931 / 5	8.4845 / 2
<i>b</i> / Å	9.089 / 4	8.8597 / 2
<i>c</i> / Å	47.117 / 11	13.8271 / 2
Cell angles		
α / °	86.28 / 3	99.702 / 2
β / °	86.44 / 4	100.861 / 2
γ / °	65.28 / 5	100.397 / 2
Cell volume <i>V</i> / Å <sup>3</sup>	3076.39	981.691
<i>Z</i>	6	2
<i>V</i> / <i>Z</i> / Å <sup>3</sup>	512.732	490.846
<i>R</i> <sub>1</sub>	0.2632	0.0407
<i>wR</i> <sub>2</sub>	0.6280	0.1079
Refln. Obs. / Unique	7202 / 1654	9530 / 3574
<i>R</i> <sub>int</sub>	0.0796	0.0117
GOF	1.351	1.100
CCDC number	1833362	1833361

*R*<sub>1</sub>: residual factor for the reflections, *wR*<sub>2</sub>: weighted sum of least squares residual of the reflections, *R*<sub>int</sub>: residual for symmetry-equivalent reflections used to calculate the average intensity margining error of refinement, GOF: least-squares goodness-of-fit parameter for all reflections included in the refinement after the final cycle of refinement, CCDC: Cambridge crystallographic data centre.

**Table 3.** Proximity of oxygen atoms and distances in **SC**.<sup>[a]</sup>

Molecule (colour) <sup>[b]</sup>	Oxygen Atoms of Ethers Proximal to Carboxyl Oxygens and Ether Oxygens						O–O Distance in Carboxylic Dimers (Å)
	O1A	O1B	O1C	O1D	O1E	O1F	
A (yellow)	—	n/a	n/a	n/a	n/a	O3A (3.5)	O2A–O3B (2.6)
B (grey)	n/a	—	O1B (4.4)	n/a	n/a	O2B (4.2)	O3A–O2B (2.5)
C (orange)	n/a	O1C (4.4)	—	n/a	O2C (4.0)	n/a	O2C–O3D (2.8)
D (cyan)	n/a	n/a	n/a	—	O3D (3.5)	n/a	O3C–O2D (2.6)
E (magenta)	n/a	O3E (3.5)	O2E (4.1)	n/a	—	n/a	O2E–O3F (2.7)
F (blue)	n/a	O2F (4.0)	O3F (3.3)	n/a	n/a	—	O3E–O2F (2.7)

[a] Numbers in parentheses indicate distances (unit: Å). “n/a” indicates none of the oxygen atoms are close to the ether oxygen indicated. Because distances were calculated by using crystallography data with an R factor of 26.3%, the values include large errors. [b] The colours indicated in parentheses represent the colour of the molecules shown in Figure 6.

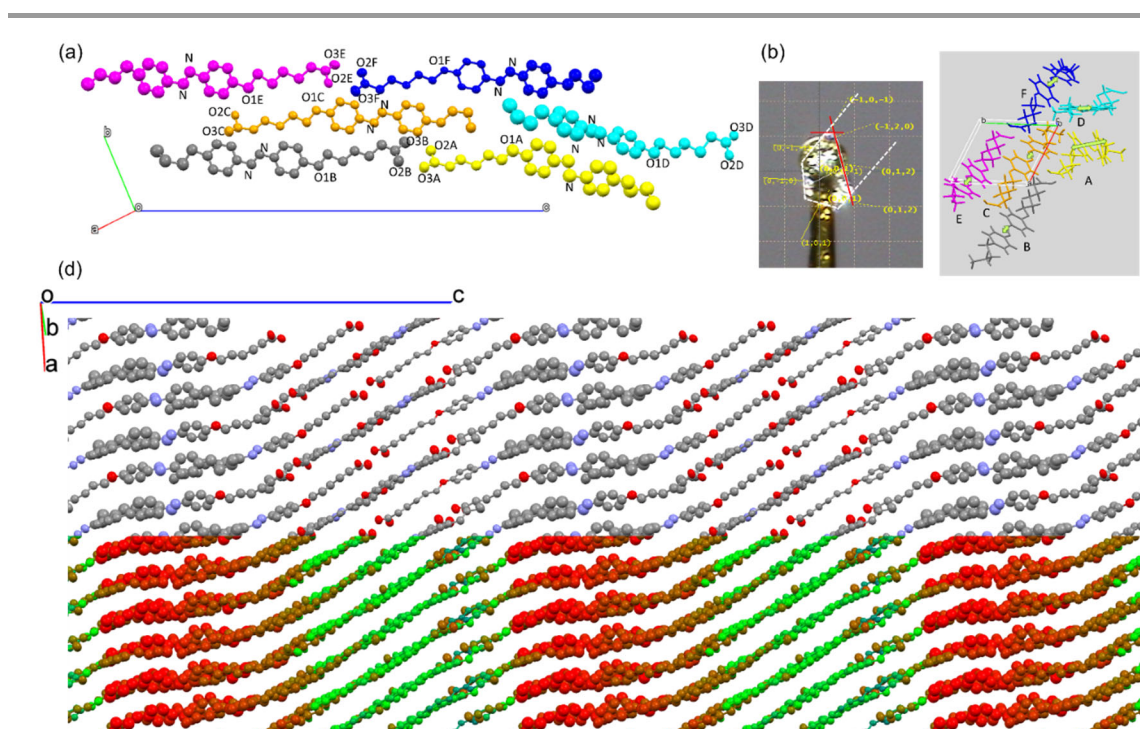


**Figure 6.** Crystal structure of **SC** measured at 93 K. (a) The unit-cell structure illustrated is ellipsoid with 50% probability. Six different colours are used to indicate independent molecules. (b) A photograph of the **SC** crystal subjected to single crystal analysis. Since the width of the crystal was sufficiently large (the edge of the crystal is indicated with a white dashed line), the crystal was cut along the lines shown in red. The long-edge of the crystal was (100) plane. (c) View of the unit-cell structure from the same direction as shown in (b). Green arrows indicate the expected transition dipole moments for  $n\text{-}\pi^*$  excitation. The transition dipole moments were calculated by using the TD-DFT method with B3LYP/6-31+G\* basis set after partial optimisation of the molecular structures as described in the experimental section. (d) Packing structure of the **SC** crystal. In the upper panel, colours indicate: carbon atoms (grey), nitrogen atoms (light blue), and oxygen atoms (red). In the lower panel, colours indicate large (red) and moderate (green) magnitudes of atomic displacement (Mercury software). The direction of the incident light is nearly parallel to the c-axis. All of the hydrogen atoms were omitted for simplicity.

### Motion of SC under polarised light

When the SC crystal described in the previous section was observed under non-polarised light, one cycle of motion included four steps (Fig. 4c). By subsequently varying the orientation of the applied polarised light in relation to the SC crystal, further insights into the dynamics of SC motion were observed. For example, when the polarisation of the incident light was applied parallel to the long axis of the crystal, a flipping motion derived from a set of single steps was observed (Fig. S3, Movie S6 in ESI). However, when the polarisation axis of the incident light was applied orthogonally to the long axis of the crystal, no sustainable motion was observed.

As briefly mentioned above, complicated flipping motions of SC with multi-mode oscillations were generally observed. When we subsequently applied various angles of polarised light to these crystals, three kinds of behaviour were revealed: (1) standstill, (2) periodic motion, and (3) inductive morphological change before 1 or 2. These experiments are presented in Movie S5. This movie is also schematically summarised in Figure 7. Thus, under non-polarised light, the crystal in its original state (shape A) transformed to shapes B, C, and D, sequentially, and back to the original structure. When steady state polarised light was applied at various angles (e.g.,  $0^\circ$  (nearly orthogonal to the long-edge of the crystal),  $30^\circ$ ,  $120^\circ$ , or  $150^\circ$ ), the crystal underwent irreversible bending or stretching to achieve shapes A, E, B, and B, respectively. Then, when the polarisation angle of the incident light was  $60^\circ$  or  $90^\circ$ , periodic motion was observed, albeit via distinct routes. For example, when polarised light was applied at  $60^\circ$ , shape E appeared between shapes D and A. When polarised light was applied at  $90^\circ$ , shape F appeared between shapes D and C. The motion and shape of the crystal were also affected by previous exposure to polarised light irradiation. For example, when polarised light was applied at  $90^\circ$  to shape A, the crystal transformed to shapes B and C before its indigenous periodic motion.

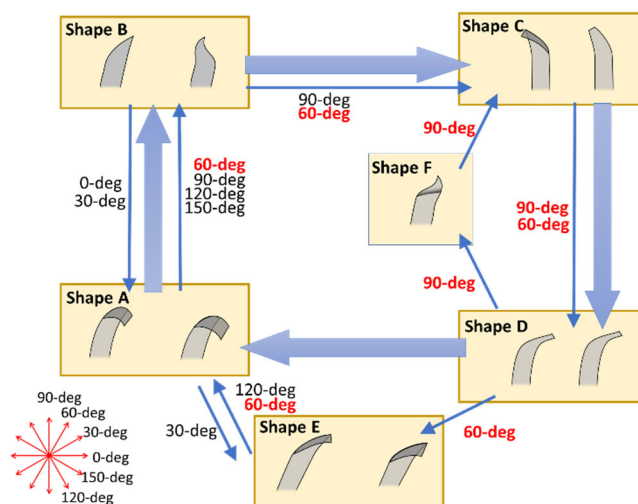


**Figure 7.** Schematic illustration of the state transitions observed in SC under non-polarised light versus various polarised light. These results are summarised from Movie S5. Thick arrows indicate the limit-cycle route under non-polarised light, while thin arrows indicate the transition which occurs under irradiation with a specific angle of polarised light. Bold red angles indicate the routes for the periodic cycle. The definition of the angle is shown at the lower-left.

### Discussion of the self-oscillatory motion of SC

Tight molecular packing in molecular assemblies of azobenzene has been shown to inhibit *trans*-to-*cis* photoisomerisation.<sup>49</sup> According to HPLC measurements, the *cis*-isomer ratio in **EC** in a photostationary state (PSS) under 435-nm light irradiation is 0.7%, while it is 28% in methanolic solution.<sup>42</sup> Meanwhile, we found the *cis*-isomer ratio in **SC** (which includes other polymorphs) to be 4.8% in a PSS in the present study (Figure S4 in ESI). Thus, we hypothesise that the soft structure of **SC** allows *trans*-to-*cis* photoisomerisation of azobenzene to occur. Furthermore, we hypothesise that specific azobenzene molecules located between durable skeleton layers are isomerised to trigger structural transitions in the **SC** crystal. As shown in Figure S3 and Movie S6 in ESI, sustainable flipping was observed under polarised light when the polarisation axis was parallel to the long-axis of the crystal (e.g., parallel to the a-axis of the crystal) (Figure 6, b and c). The lowest excitation transition dipole moments of each independent azobenzene were calculated in the crystal (Figure 6c). However, the accuracy of these calculations are limited due to flexibility of the azobenzene molecules in the crystal. Azobenzene molecules E and F (coloured magenta and blue, respectively, in Figure 6), satisfied both conditions of movability and stable direction of transition moment for *trans*-to-*cis* isomerisation under polarised light. Thus, we predict that photoisomerisation of these molecules plays a key role in inducing self-oscillation as a dominant mode. Moreover, considering the average percentage of the *cis*-isomer in the PSS (4.8%), the threshold for a structural transition from the original state to a metastable alignment is estimated to involve one *cis*-isomer in two crystalline unit cells. However, this value has not been confirmed because we have not yet determined the structures of the generated assembly. Moreover, since it is assumed that the bent crystal represents a mixture of the original alignment domain and the generated alignment domain, the threshold for the number of *cis*-isomers in each unit cell which achieve a transition state may be higher.

#### **Estimated structure of coC and its dynamics**

Preparation of **coC** was easier than that for **SC**. As shown in Figure S1f-i, 1D-XRD patterns for the samples obtained after cooling down ultrasonicated dispersions of **1** and **2** were generally simpler than the pattern obtained for the dispersion of **1**. When the ultrasonicated mixture was kept at 55 °C, **EC** was obtained along with non-crystalline assemblies such as vesicles. This result suggests that when **2** and **1** co-exist at temperatures cooler than room temperature, formation of a single component assembly of **1** is inhibited. When small-angle pXRD patterns of **SC** in its original state were calculated from a single-crystal XRD analysis (Figures 3c and S1d), the (001) and (005) peaks were strong, whereas the (002) and (004) peaks were weak. For the **coC** crystal, the 1D-XRD (001), (003), and (005) peaks were observed at similar 2 $\theta$  values as observed for **SC** (Figure S1g-i). Taken together, these results suggest that the molecular alignments of **SC** and **coC** are similar, despite differences in their components. Based on two observations, 1) the component ratio of **1** and **2** is nearly 6:4 in **coC**<sup>42</sup> and 2) ether oxygen atoms play a role in forming a dense-layer of azobenzene molecules which interact with carboxyl groups in **SC**, we can assume that two of the six azobenzene molecules in **SC** (molecules A and D, coloured yellow and cyan, respectively, in Figure 6) are substituted by oleic acid in **coC**. Meanwhile, molecules E and F in **SC** (coloured magenta and blue, respectively, in Figure 6), which are located in the sparse layer, undergo photoisomerisation to trigger a phase transition and induce a flipping motion in **coC**. Accordingly, the flipping behaviour should depend on the polarisation angle of incident light. This was in fact observed with **coC** (see Figure 8), such that the self-oscillatory motion of **coC** is dependent on the polarisation angle of the

applied irradiation. For example, when polarised light was applied at angles of 120° or 135°, the crystal underwent oscillatory flipping, yet it did not exhibit periodical motion when polarised light was applied orthogonal to the crystal. This represents an important insight into this system, since a relationship between the axis and shape of a crystalline structure was not previously determined.<sup>50</sup>

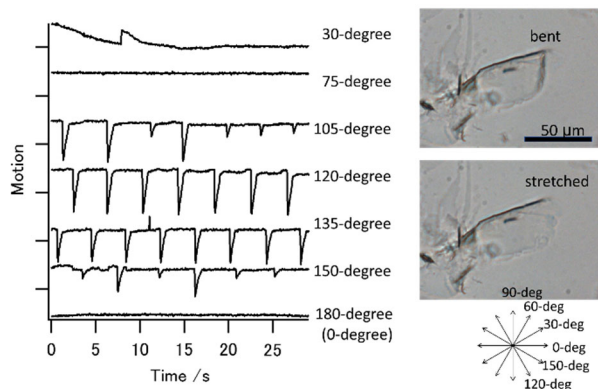


**Figure 8.** The motion observed for **coC** under polarised-light irradiation ( $\lambda = 435$  nm). (Left) Time-course of the motion. The vertical axis indicates the brightness of a small area indicated in the micrograph. Because we could not use DIC optics, the micrographs are not clear. In addition, the tracking method for the time-course chart was changed from that used in Figure 5. The crystal bent just before the line descending and was maintained in this state even after the line returned to its original level. Stretching motion with a phase transition occurred while the line was flattened. The irregular curve detected under 30° polarised light shows a phase transition. Repetitive phase transitions were not observed. (Right) Micrographs of the flipping motion observed under 120° polarised light.

#### Discussion of multi-mode oscillation

Compared to **coC**,<sup>42</sup> the periodic flips exhibited by **SC** tended to be more complicated, even under non-polarised light. This may be due to various azobenzene molecules within the crystal undergoing photoisomerisation during the self-oscillatory cycle. Azobenzene molecules which do not generate the dominant oscillation by triggering a phase transition may potentially serve as a generator for another periodic motion. However, this hypothesis has low probability because it has been shown that a collective reaction to attain periodic dynamics is an inherently rare phenomenon. Thus, we consider that modulation of periodicity could be mediated by one azobenzene molecule acting as an oscillation generator. We present a model in Figure 9 to explain this possibility. In this model, X represents an azobenzene molecule which causes a phase transition, while Y is an azobenzene molecule which is not susceptible to phase transition due to its location.

Under blue-light irradiation, *trans*-to-*cis* photoisomerization of X occurs. When the isomer-ratio becomes  $\beta$ , a phase transition is triggered and the crystal changes to shape B. In shape B, *cis*-to-*trans* photoisomerization can then occur. For molecules of Y which do not exhibit this behaviour (as shown in Fig. 2), when the isomer-ratio of X becomes  $\alpha$ , a reverse phase transition occurs.

Next, we considered if Y affects periodic motion. In the initial crystal, the isomer-ratios of X and Y are  $\alpha$  and  $a$ , respectively. When the isomer-ratio of X becomes  $\beta$  under blue-light irradiation, the isomer-ratio of Y changes to  $b$ . Then, phase transition occurs. In shape B, reverse photoisomerization of X is expected, while reverse photoisomerization of Y is not guaranteed. In the example shown in Figure 9, when the isomer ratio of X becomes  $\gamma$  (for simplicity, we can regard



For **coC**, although it exhibits a similar motion to **SC**, the changes triggered in it by polarised light are too complicated to rationalise with a simple rule. It was frequently observed that the **coC** crystal cleaved, melted, and kept its curled form. We hypothesise that this behaviour is due to the presence of weaker molecular interactions in **coC** than in **SC**. There were only two modes associated with the observed periodic motions of **SC**, an alternately swinging motion in two different directions and a single-mode flipping motion (see Movie S7 in the present study and previously published videos<sup>42</sup>). Both of these motions were observed under non-polarised light, while the single-mode motion was frequently observed if the crystals had sufficient thickness. When we observed the alternately swinging motion, selective generation of a singular oscillation was successful when polarised light was applied. Meanwhile, selective generation of the other mode was never successful (Movie S7 and Figure S5). This result may be due to the fact that both swinging motions are generated by the same oscillation generator, and one of the motions derives from regulation by another azobenzene molecule. We illustrate these proposed mechanisms in Figure 9. The existence of simpler modes in **coC** compared to those in **SC** is presumably due to the small modulation effect induced by non-photoreactive molecules compared with azobenzene molecules in these two assemblies, respectively.

## Conclusion

Here, we describe the autonomous flipping motion in response to light energy observed in a crystal containing azobenzene derivative **1** without oleic acid (**2**). Based on similarities in the mechanical dynamics and molecular alignment of **SC** and **coC**, we conclude that both crystals employ the same mechanism<sup>51</sup> whereby a limit-cycle self-oscillatory motion is spatially governed by a bi-stable crystalline structure and the frequency of the motion depends on the number of photons received. Furthermore, in the present study, we reveal that **SC** has a sparse-and-dense mille-feuille-like layered structure, according to single-crystal XRD data collected at 93 K. Based on the crystal structure and motions observed under polarized light, we predict that: (1) the molecules in the dense layer prevent decomposition of the crystal, (2) the sparse structure allows repetitive photoisomerisation events to occur, and the efficiency of these events depend on molecular crowding in the crystal and the relative angle of the light source, and (3) a specific molecule in the sparse layer generates the self-oscillation motion shown in Figure 2, while the other molecules contribute to an auxiliary mode of oscillation. However, we cannot exclude the possibility that these complicated dynamics are a result of synchronisation among multiple self-oscillating molecules.

Thus, the results of the present study demonstrate that the self-organised motion observed in an azobenzene crystal is due to a limit-cycle which is established based on a relationship between molecular alignment and the parameters of an applied light. Accordingly, the autonomous behaviour observed represents a response to the information contained in the supplied energy source or environment, and the motion becomes rich in variety. Therefore, while stimulus-responsive materials change their morphology to attain a static structure, we describe here an autonomous material which converts accepted information into a spatio-temporal pattern. Furthermore, while both types of materials can respond to environmental conditions, the latter provides support for constructing self-governable molecular robots.

## Acknowledgements

The authors thank Prof. Masako Kato and Prof. Atsushi Kobayashi for the 1D-XRD measurement. This work was supported by JST PRESTO “Molecular Technology and Creation of New Functions” (Grant Number, JPMJPR13K6), by JSPS KAKENHI (Grant Number, JP17H05247) in Scientific Research on Innovative Areas “Photosynergetics”, and by JSPS KAKENHI (Grant Number, JP18H05423) in Scientific Research on Innovative Areas “Molecular Engine”.

## Conflicts of interest

The authors have no conflicts of interest to declare.

## References

1. Yewdall, N. A.; Mason, A. F.; Hest, J. C. M. v., The hallmarks of living systems: towards creating artificial cells. *Interface Focus* **2018**, *8* (5), 20180023.
2. Fialkowski, M.; Bishop, K. J. M.; Klajn, R.; Smoukov, S. K.; Campbell, C. J.; Grzybowski, B. A., Principles and Implementations of Dissipative (Dynamic) Self-Assembly. *J. Phys. Chem. B* **2006**, *110* (6), 2482-2496.
3. Grzybowski, B. A.; Huck, W. T. S., The nanotechnology of life-inspired systems. *Nat. Nanotechnol.* **2016**, *11* (7), 585-592.
4. Kageyama, Y., Light-Powered Self-Sustainable Macroscopic Motion for the Active Locomotion of Materials. *ChemPhotoChem* **2019**, *3* (6), 327-336.
5. Merindol, R.; Walther, A., Materials learning from life: concepts for active, adaptive and autonomous molecular systems. *Chem. Soc. Rev.* **2017**, *46* (18), 5588-5619.
6. Ragazzon, G.; Prins, L. J., Energy consumption in chemical fuel-driven self-assembly. *Nat. Nanotechnol.* **2018**, *13* (10), 882-889.
7. Boekhoven, J.; Hendriksen, W. E.; Koper, G. J. M.; Eelkema, R.; van Esch, J. H., Transient assembly of active materials fueled by a chemical reaction. *Science* **2015**, *349* (6252), 1075-1079.
8. van Rossum, S. A. P.; Tena-Solsona, M.; van Esch, J. H.; Eelkema, R.; Boekhoven, J., Dissipative out-of-equilibrium assembly of man-made supramolecular materials. *Chem. Soc. Rev.* **2017**, *46* (18), 5519-5535.
9. Morrow, S. M.; Colomer, I.; Fletcher, S. P., A chemically fuelled self-replicator. *Nat. Commun.* **2019**, *10* (1), 1011.
10. Astumian, R. D., How molecular motors work – insights from the molecular machinist's toolbox: the Nobel prize in Chemistry 2016. *Chem. Sci.* **2017**, *8* (2), 840-845.
11. Danowski, W.; van Leeuwen, T.; Abdolahzadeh, S.; Roke, D.; Browne, W. R.; Wezenberg, S. J.; Feringa, B. L., Unidirectional rotary motion in a metal–organic framework. *Nat. Nanotechnol.* **2019**, *14* (5), 488-494.
12. Sun, Z.; Yamauchi, Y.; Araoka, F.; Kim, Y. S.; Bergueiro, J.; Ishida, Y.; Ebina, Y.; Sasaki, T.; Hikima, T.;

- Aida, T., An Anisotropic Hydrogel Actuator Enabling Earthworm-Like Directed Peristaltic Crawling. *Angew. Chem. Int. Ed.* **2018**, *57* (48), 15772-15776.
13. Hosono, N.; Kajitani, T.; Fukushima, T.; Ito, K.; Sasaki, S.; Takata, M.; Aida, T., Large-Area Three-Dimensional Molecular Ordering of a Polymer Brush by One-Step Processing. *Science* **2010**, *330* (6005), 808-811.
  14. Iamsaard, S.; Asshoff, S. J.; Matt, B.; Kudernac, T.; Cornelissen, J. J.; Fletcher, S. P.; Katsonis, N., Conversion of light into macroscopic helical motion. *Nat. Chem.* **2014**, *6* (3), 229-35.
  15. Yu, Y. L.; Nakano, M.; Ikeda, T., Directed bending of a polymer film by light - Miniaturizing a simple photomechanical system could expand its range of applications. *Nature* **2003**, *425* (6954), 145-145.
  16. Yotsuji, H.; Higashiguchi, K.; Sato, R.; Shigeta, Y.; Matsuda, K., Phototransformative Supramolecular Assembly of Amphiphilic Diarylethenes Realized by a Combination of Photochromism and Lower Critical Solution Temperature Behavior. *Chem. Eur. J.* **2017**, *23* (60), 15059-15066.
  17. Sakaguchi, A.; Higashiguchi, K.; Matsuda, K., Anisotropic Diffusion of Microbeads Surrounded by an Anisotropically Elongated Supramolecular Diarylethene Architecture under Linearly Polarized Light. *ChemPhotoChem* **2017**, *1* (11), 488-492.
  18. Higashiguchi, K.; Taira, G.; Kitai, J.; Hirose, T.; Matsuda, K., Photoinduced macroscopic morphological transformation of an amphiphilic diarylethene assembly: reversible dynamic motion. *J. Am. Chem. Soc.* **2015**, *137* (7), 2722-9.
  19. Kageyama, Y.; Ikegami, T.; Kurokome, Y.; Takeda, S., Mechanism of Macroscopic Motion of Oleate Helical Assemblies: Cooperative Deprotonation of Carboxyl Groups Triggered by Photoisomerization of Azobenzene Derivatives. *Chem. Eur. J.* **2016**, *22* (25), 8669-8675.
  20. Kageyama, Y.; Tanigake, N.; Kurokome, Y.; Iwaki, S.; Takeda, S.; Suzuki, K.; Sugawara, T., Macroscopic motion of supramolecular assemblies actuated by photoisomerization of azobenzene derivatives. *Chem. Commun.* **2013**, *49* (82), 9386-9388.
  21. Chen, J. W.; Leung, F. K. C.; Stuart, M. C. A.; Kajitani, T.; Fukushima, T.; van der Giessen, E.; Feringa, B., Artificial muscle-like function from hierarchical supramolecular assembly of photoresponsive molecular motors. *Nat. Chem.* **2018**, *10* (2), 132-138.
  22. Hamada, T.; Sugimoto, R.; Vestergaard, M. C.; Nagasaki, T.; Takagi, M., Membrane Disk and Sphere: Controllable Mesoscopic Structures for the Capture and Release of a Targeted Object. *J. Am. Chem. Soc.* **2010**, *132* (30), 10528-10532.
  23. Hamada, T.; Sato, Y. T.; Yoshikawa, K.; Nagasaki, T., Reversible photoswitching in a cell-sized vesicle. *Langmuir* **2005**, *21* (17), 7626-7628.
  24. Kitagawa, D.; Tanaka, R.; Kobatake, S., Photoinduced stepwise bending behavior of photochromic diarylethene crystals. *CrystEngComm* **2016**, *18* (38), 7236-7240.
  25. Kobatake, S.; Takami, S.; Muto, H.; Ishikawa, T.; Irie, M., Rapid and reversible shape changes of molecular crystals on photoirradiation. *Nature* **2007**, *446*, 778.

26. Koshima, H.; Ojima, N.; Uchimoto, H., Mechanical Motion of Azobenzene Crystals upon Photoirradiation. *J. Am. Chem. Soc.* **2009**, *131* (20), 6890-6891.
27. Morimoto, M.; Irie, M., A Diarylethene Cocrystal that Converts Light into Mechanical Work. *J. Am. Chem. Soc.* **2010**, *132* (40), 14172-14178.
28. Irie, M., Photochromism and molecular mechanical devices. *Bull. Chem. Soc. Jpn.* **2008**, *81* (8), 917-926.
29. Yoshida, R.; Ueki, T., Evolution of self-oscillating polymer gels as autonomous polymer systems. *Npg Asia Mater.* **2014**, *6*.
30. Yoshida, R., Development of self-oscillating polymers and gels with autonomous function. *Polym. J.* **2010**, *42* (10), 777-789.
31. Uchida, E.; Azumi, R.; Norikane, Y., Light-induced crawling of crystals on a glass surface. *Nat. Commun.* **2015**, *6*, 7310.
32. Yamada, M.; Kondo, M.; Mamiya, J.; Yu, Y.; Kinoshita, M.; Barrett, C.; Ikeda, T., Photomobile polymer materials: Towards light-driven plastic motors. *Angew. Chem. Int. Ed.* **2008**, *47* (27), 4986-4988.
33. Wie, J. J.; Shankar, M. R.; White, T. J., Photomotility of polymers. *Nat. Commun.* **2016**, *7*, 13260.
34. Gelebart, A. H.; Jan Mulder, D.; Varga, M.; Konya, A.; Vantomme, G.; Meijer, E. W.; Selinger, R. L. B.; Broer, D. J., Making waves in a photoactive polymer film. *Nature* **2017**, *546*, 632-636.
35. Ge, F.; Zhao, Y., A new function for thermal phase transition-based polymer actuators: autonomous motion on a surface of constant temperature. *Chem. Sci.* **2017**, *8* (9), 6307-6312.
36. Serak, S.; Tabiryan, N.; Vergara, R.; White, T. J.; Vaia, R. A.; Bunning, T. J., Liquid crystalline polymer cantilever oscillators fueled by light. *Soft Matter* **2010**, *6* (4), 779-783.
37. White, T. J.; Tabiryan, N. V.; Serak, S. V.; Hrozhyk, U. A.; Tondiglia, V. P.; Koerner, H.; Vaia, R. A.; Bunning, T. J., A high frequency photodriven polymer oscillator. *Soft Matter* **2008**, *4* (9), 1796-1798.
38. Vantomme, G.; Gelebart, A. H.; Broer, D. J.; Meijer, E. W., Self-sustained actuation from heat dissipation in liquid crystal polymer networks. *J. Polym. Sci. A: Polym. Chem.* **2018**, *56* (13), 1331-1336.
39. Vantomme, G.; Gelebart, A. H.; Broer, D. J.; Meijer, E. W., A four-blade light-driven plastic mill based on hydrazone liquid-crystal networks. *Tetrahedron* **2017**, *73* (33), 4963-4967.
40. Gelebart, A. H.; Vantomme, G.; Meijer, E. W.; Broer, D. J., Mastering the Photothermal Effect in Liquid Crystal Networks: A General Approach for Self-Sustained Mechanical Oscillators. *Adv Mater* **2017**, *29* (18), 1606712.
41. Nicolis, G.; Prigogine, I., Nonlinear Thermodynamics. In *Self-Organization in Nonequilibrium Systems From Dissipative Structure to Order through Fluctuations*, ed.; John Wiley & Sons, Inc.: New York, 1977; pp 49-60.
42. Ikegami, T.; Kageyama, Y.; Obara, K.; Takeda, S., Dissipative and Autonomous Square-Wave Self-Oscillation of a Macroscopic Hybrid Self-Assembly under Continuous Light Irradiation. *Angew.*

*Chem. Int. Ed.* **2016**, *55*, 8239-8243.

43. Haken, H., *Synergetics - An Introduction* (Japanese transl.) ed.; Springer-Verlag: Berlin Heidelberg, 1978.
44. Only when the direction of polarized light was parallel to the analyzer of the DIC optics, we were able to record the movie. Else, we recorded motion without using the DIC optics.
45. M. J. Frisch, et al., Gaussian 16, Revision B.01, Gaussian, Inc., Wallingford CT, 2016.
46. Kageyama, Y.; Ikegami, T.; Hiramatsu, N.; Takeda, S.; Sugawara, T., Structure and growth behavior of centimeter-sized helical oleate assemblies formed with assistance of medium-length carboxylic acids. *Soft Matter* **2015**, *11* (18), 3550-3558.
47. All polymorphs of crystals dissolved under UV-light (365 nm wavelength) irradiation.
48. The ratio of the absorption coefficients of 1-trans/1-cis is larger at 435 nm than at 470-nm (measured in methanolic solution). see ref. 42
49. Matsumoto, M.; Terrettaz, S.; Tachibana, H., Photo-induced structural changes of azobenzene Langmuir-Blodgett films. *Adv. Colloid Interface Sci.* **2000**, *87* (2-3), 147-164.
50. An assumable structure of **coC**, and another example of flippings of **coC** under polarized light is shown in Figure S5 in ESI.
51. It is noteworthy that the mechanism depends on the molecular structure and alignments: different-type periodic motion was reported in the ribbon-shape assembly composed of **1**, **2** and stearic acid. See ref. 42

## Supplementary Information

### Table of Contents

- Figure S1.** Powder XRD patterns of various crystals (p. S3)
- Figure S2.** Structure of an EC crystal obtained from an ethanol solution (p. S4)
- Figure S3.** Self-oscillatory motion of SC under polarised light (p. S5)
- Figure S4.** HPLC analysis of crystals after 435-nm light irradiation (p. S6)
- Figure S5.** Self-oscillatory motion of coC under polarised light (p. S7)
- Movie S1.** Self-oscillation motion observed in a SC crystal under 435-nm light irradiation.  
A single component crystal of azobenzene derivative (1) exhibited a self-exciting periodic flipping motion under continuous 435-nm light irradiation. The frequency of oscillation increased with greater light intensity.
- Movie S2.** Self-oscillation motion observed in a SC crystal under 470-nm light irradiation.  
The crystal shown in movie S1 also exhibited a self-exciting periodic flipping motion under continuous 470-nm light irradiation. The frequency of oscillation increased with greater light intensity.
- Movie S3.** A variety of self-oscillatory motions observed in other SC crystals under 435-nm light.
- Movie S4.** A variety of self-oscillatory motions observed in other SC crystals under 470-nm light.
- Movie S5.** Self-oscillatory motions of a SC crystal under polarised light (1).  
Multi-step flips of SC molecules under non-polarised and polarised light irradiation are shown.

**Movie S6.** Self-oscillatory motions of a **SC** crystal under polarised light (2).

Angular motion and simpler flips of a **SC** molecule observed under polarised light irradiation.

**Movie S7.** Self-oscillatory motions of a **coC** crystal under polarised light.

Multi-step flips of **coC** molecules in response to various polarisation states of light are shown.

(Movies were not uploaded to the preprint server.)

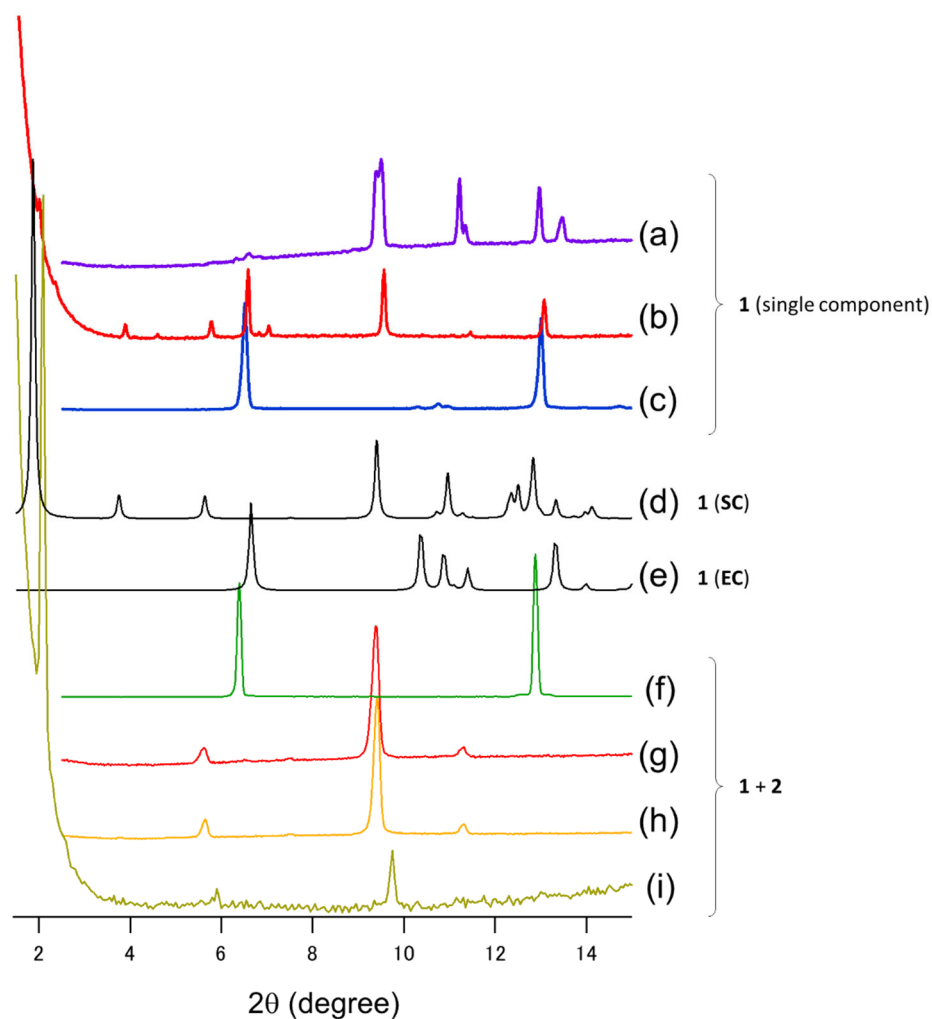
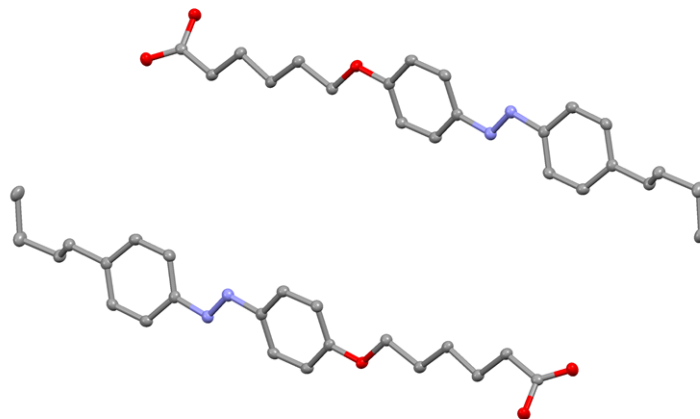


**Figure S1.** Under aqueous conditions, 1D-XRD patterns were measured with a  $\text{CuK}\alpha$  source and pXRD patterns were calculated from single crystal XRD analysis. The vertical axis represents x-rays in arbitrary units. (a-c) Profiles from 1D-XRD performed for crystals in an aqueous dispersion of **1**: (a) prepared by cooling an 85 °C dispersion (NC), (b) prepared by cooling a boiled dispersion (mixture of SC, EC, and other polymorphs), and (c) prepared by incubating the aqueous dispersion at 55 °C after ultrasonication at 55 °C. pXRD patterns calculated for a SC crystal of **1** (d) and an EC crystal of **1** (e). (f-i) 1D-XRD patterns are shown for crystals prepared from an aqueous dispersion of **1** and **2**. Crystals were prepared with ultrasonication at 55 °C and then were maintained at 55 °C (f). Crystals were prepared with ultrasonication at 55 °C, followed by an incubation at 0 °C for 30 min (g). Crystals were prepared by incubating the mixture at room temperature after an ultrasonication step at 55 °C (h and i). Measurements were made with a Miniflex600 (Rigaku) system (a, c, and f-h), a D8 Advance (Bruker) system (b), and a RINT2000 (Rigaku) system (i). The  $2\theta$  values include errors which are attributed to the XRD equipment not being optimised for aqueous samples.

(a) Unit cell structure



(b) Packing structure

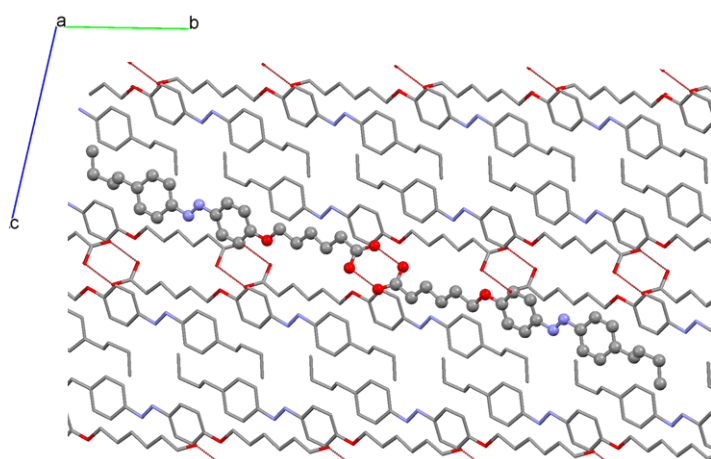


**Figure S2.** Crystal structure of **EC** revealed by single crystal XRD operated at 293 K. Colours indicate the elements present (grey for carbon, light blue for nitrogen, and red for oxygen). (a) The unit cell structure (ellipsoid with 50% probability) and (b) packing structure (red lines indicate hydrogen bonds between carboxylic acids) are shown. Hydrogen atoms were omitted to simplify visualisation of the models.

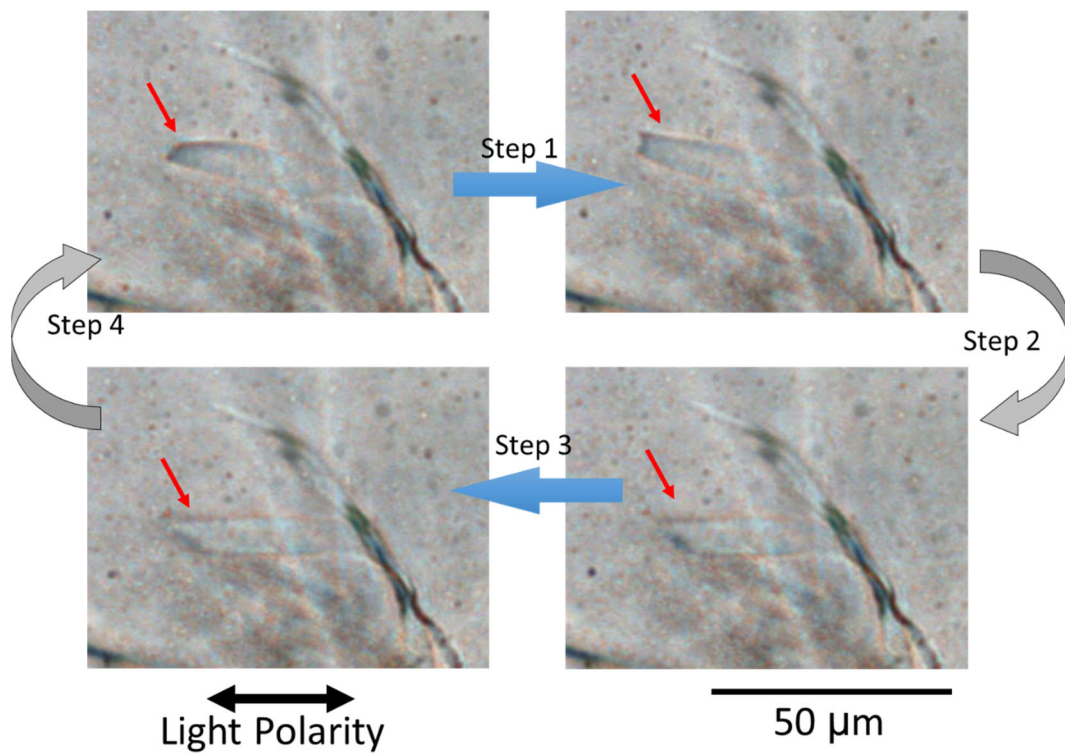


**Figure S3.** Micrographs of the periodic motion of SC (indicated with red arrows) under light polarised in the horizontal direction, captured from Movie S6. The angle of the polarised light ranged from  $0^\circ$  to  $30^\circ$  in relation to the long axis of the crystal. These images provide examples of the simple motions which occurred compared with the motions shown in Figure 7 (Movie S5).

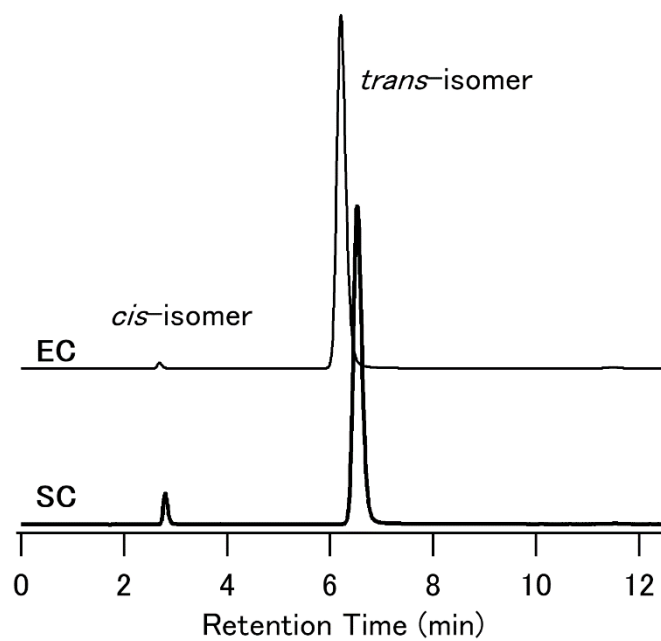


**Figure S4.** HPLC charts for **EC** (gray line) and **SC** (black line) after 435-nm light irradiation is applied until the system attained a photostationary state.

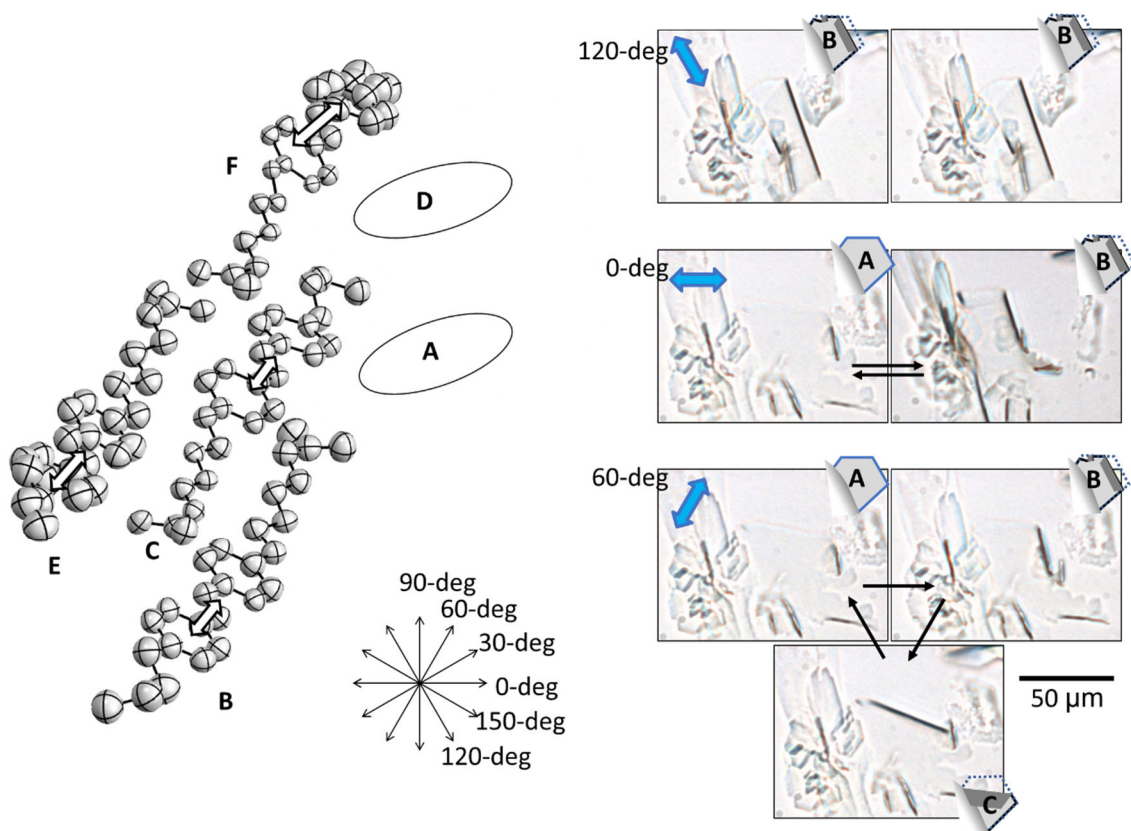


**Figure S5.** (Left) Molecular modelling of **coC** based on the crystal structure of **SC**. Molecules **A** and **D** are substituted to oleic acid (**2**) and molecules **B**, **D**, **E**, and **F** are azobenzene derivative (**1**). (Right) Still frame images from Movie S7 of a thin **coC** under variable polarised light. Under  $120^\circ$  and  $150^\circ$  polarised light, the crystal kept its initial structure. (In the movie, shape **B** of the crystal was irradiated.) Under  $0^\circ$  polarised light, single-mode oscillatory flipping was realised. Under  $30^\circ$ ,  $60^\circ$ , and  $90^\circ$  polarised light, three stages of the oscillatory flipping cycle were observed. Based on the recorded observations, no single-mode oscillation between **A** and **C** appeared.